

Effects of finite trapping on the decay, recoil, and decoherence of dark states of quantum emitter arrays

M. Eltohfa^{1,*} and F. Robicheaux^{1,2,†}

¹*Department of Physics and Astronomy, Purdue University, West Lafayette, Indiana 47906 USA*

²*Purdue Quantum Science and Engineering Institute,
Purdue University, West Lafayette, Indiana 47907, USA*

(Dated: February 17, 2025)

The collective interaction of electronic excitations with the electromagnetic field in atomic arrays can lead to significantly reduced decay rates, resulting in the formation of subradiant states with promising applications in quantum information and quantum memories. In many previous studies, atoms are assumed to be perfectly positioned and fixed. In this work, we investigate the effects of finite trap strength on the long-lived subradiant states for two, three, and many atoms in a 1D waveguide or free space. We demonstrate that the decay rate is lower bounded by the spatial spread of the motional wavefunction, which is non-zero even for the vibrational ground state. Additionally, in relatively tight traps, the decay of a shared electronic excitation imparts recoil energy to the atoms, which is proportional to the lifetime of the excited state[1]. In a 1D waveguide, this energy can reach a vibrational quantum, even in the Lamb-Dicke regime. Furthermore, for atoms in weaker traps, the induced dipole forces become significant, causing the atoms to undergo motion prior to decay. This motion results in a time-dependent decay rate, an additional energy transfer to the atoms following decay, and mixing between the different electronic eigenstates. Consequently, these effects lead to decoherence and a reduction in the fidelity of a stored electronic eigenstate. Infidelity can be mitigated by either decreasing the induced forces or increasing the trap strength. For quantum information storage, these considerations suggest optimal array configurations, both in terms of geometric arrangements and polarization directions. Our findings provide insights for the behavior of quantum memories and atom array experiments.

I. INTRODUCTION

Achieving controlled coupling between light and matter is essential for coherent quantum control and quantum information processing. To enable this, one of the tools is to utilize the collective interaction between atoms by placing them close to each other [2, 3]. Compared to individual decay rates, collective emission rates can be significantly enhanced or suppressed [4–10]. In circular atomic arrays with subwavelength separations, for example, the decay rate of the excitation eigenstates decreases exponentially with the number of atoms [11], which is useful for the storage of photons.

Furthermore, the collective decay can be used to control the radiation pattern or the direction of the emitted photons [12–14]. For example, the radiation could be suppressed to all but one selected channel where the atoms radiate efficiently [15]. Another example is that the geometry of a 2D array of atoms can be optimized such that the array acts like a perfect mirror [16, 17]. Additionally, the smaller decay rate of the subradiant or dark states results in the emitted light spectrum having a narrower linewidth. This is utilized for collective cooling of atoms to their motional ground state better than individual atom cooling [18].

Most of the theoretical studies of collective decay assume that atoms are perfectly localized and fixed in

space. While this assumption captures many of the collective effects mentioned above, it does not directly deal with motional aspects of the atoms such as recoil due to photon emissions and decoherence due to the vibrations which are present in experiment.

Because the cooperative decay dynamics depends on the separation between the atoms, several detrimental properties could arise: 1) perfectly dark states are impossible; the excitation will necessarily have a minimum decay rate that arises from the spread in the position of the atoms [18, 19]. 2) if the atoms are placed very close together, there could be cooperative forces that impart momentum and move the atoms from their initial positions [20]. 3) the induced dipole forces can also introduce entanglement between the internal and motional degrees of freedom leading to unwanted decoherence for the internal degrees of freedom [20, 21]. This, for example, will affect the fidelity of the long-time stored photons introduced in Ref. [11]. 4) a long lifetime of a dark state is usually accompanied by large recoil after photon emission [1, 20]. 5) the imparted momentum during decay (due to the induced forces) leads to additional energy that can lead to undesired heating of a cold atom array. This heating would necessitate additional cooling steps each time the array is manipulated.

In this work, we aim to address these issues. By including the vibrational aspects of the atoms, we give quantitative results and scaling behavior of the effects of finite traps on 1) the decay rate and behavior of highly subradiant states 2) the accompanied energy *before* and *after* the emission of a photon 3) the decoherence and infidelity

* meltohfa@purdue.edu

† robichf@purdue.edu

of a dark state arising due to the induced forces.

II. METHODS

In this section, we describe the theoretical framework used to study the collective decay of atoms. Our system is the same as that described in Refs. [1, 20, 22]. To account for the motion of the atoms and the internal states, we use a density matrix formalism expanded in the vibrational states for the atoms' motion and the internal states, similar to the formalism in Ref. [20]. To study the evolution of highly subradiant states, it is sufficient to consider internal states with at most one excitation. This assumption is justified because the singly excited subspace can contain many subradiant states [15]. Moreover, we note that we do not have any driving fields such as a laser term. We assume the initial state has been prepared by some mechanism for $t < 0$ in an electronically excited state at $t = 0$.

A. System

We consider N atoms of equal mass m . Each atom i has two internal states, $|g_i\rangle$ and $|e_i\rangle$, with a transition frequency ω_0 and a spontaneous decay rate γ_0 . The operators σ_i^+ and σ_i^- are the raising and lowering operators of the internal states of atom i : $\sigma_i^+ = |e_i\rangle\langle g_i|$ and $\sigma_i^- = |g_i\rangle\langle e_i|$.

Each atom is trapped in a harmonic well. The location of the center of the trap of atom i is denoted by \mathbf{R}_i , while the location of the atom i relative to its trap center is \mathbf{r}_i . For the relative position of two traps, we use the notation $\mathbf{R}_{ij} = \mathbf{R}_i - \mathbf{R}_j$ and the relative displacement as $\mathbf{r}_{ij} = \mathbf{r}_i - \mathbf{r}_j$. We also use the absolute position of an atom which is denoted by $\tilde{\mathbf{r}}_i = \mathbf{R}_i + \mathbf{r}_i$, with corresponding difference of two atoms $\tilde{\mathbf{r}}_{ij} = \tilde{\mathbf{r}}_i - \tilde{\mathbf{r}}_j$. A schematic of the system is shown in Fig. 1. For simplicity, the traps are of equal angular frequency ω_t and evenly separated by a distance $d = |\mathbf{R}_{i+1} - \mathbf{R}_i|$. The eigenstates of the trap for atom i in each direction are denoted by $|n_i\rangle$ with energy $n_i\hbar\omega_t$ (where the conventional 1/2 is dropped for convenience).

The density matrix of the system, ρ , can be expanded in the tensor product basis of the vibrational and internal states for each atom. We denote such a generic basis state by $|A, V\rangle$ where A and V are the collection of the internal and vibrational quantum numbers of the system, respectively: $|A\rangle = |\alpha_1, \alpha_2, \dots\rangle$, and $|V\rangle = |n_1, n_2, \dots\rangle$, where at most one α_j can be e_j while the others in g_j . In this way, there are $N + 1$ allowed internal states. Each n_j can be $0, 1, 2, \dots$. Hence, the density matrix can be written as

$$\rho = \sum_{A, V} \sum_{A', V'} \rho_{A, V, A', V'} |A, V\rangle \langle A', V'|. \quad (1)$$

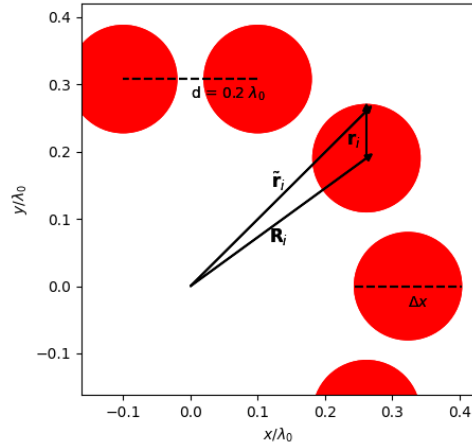


FIG. 1: Schematic of part of an atom array on a circle. Here, the atoms are trapped regularly with separation $d = 0.2\lambda_0$. The size of the red circle (Δx) indicates the spread of the trap ground state for $\eta = 1.0$. A large η was chosen for clarity. Position vectors to the center of the traps, \mathbf{R}_i , and the absolute position of the atoms, $\tilde{\mathbf{r}}_i$, as well as the relative position, \mathbf{r}_i , are shown.

For numerical feasibility, we can truncate the vibrational states to $0, 1, 2, \dots, n_{max}$, where we choose a phonon cut-off, n_{max} , to insure convergence of the numerical simulation. This way, we have $N_{vib} = n_{max} + 1$ vibrational states per atom. The vibrational Hilbert space will, therefore, contain $(N_{vib})^N$ states. The total number of states in the system is $N_{tot} = (N_{vib})^N (N + 1)$.

B. Master Equation

The evolution of the system's density matrix, ρ , is governed by a master equation

$$\frac{d\rho(t)}{dt} = -\frac{i}{\hbar} [H_{\text{eff}}\rho(t) - \rho(t)H_{\text{eff}}^\dagger] + \mathcal{R}[\rho(t)]. \quad (2)$$

where H_{eff} is an effective Hamiltonian that contains a trap term and a non-Hermitian interaction term, and \mathcal{R} is a population recycling superoperator [18] defined below. The trap term is given by

$$H_{\text{trap}} = \sum_{i=1}^N \hbar\omega_t a_i^\dagger a_i. \quad (3)$$

where a_i is the lowering operator of the vibrational states of the trap of atom i . The interaction term comes from the coupling with the electromagnetic field (which is traced out) and is given by

$$H_{\text{int}} = -\hbar \sum_{i,j} g(\tilde{\mathbf{r}}_{ij}) \sigma_i^+ \sigma_j^-, \quad (4)$$

where g is a complex valued Green's function proportional to the electric field propagator and is given in Eqs. (7) and (8) below. The imaginary part of this Green's function gives a non-Hermitian interaction responsible for the collective decay of the excited state. On the other hand, the real part gives a Hermitian interaction responsible for the collective Lamb shifts of the energy of the states and also the induced forces which can shift the positions of the atoms before the decay of the excited state [7].

The final term in Eq. (2) is the recycling superoperator, \mathcal{R} , which accounts for the decayed population and the recoil energy during the photon emission step. The recycling superoperator acts on the density matrix in a relatively complicated way. The simplest description is in the position representation of the density matrix, where ρ is expanded as

$$\rho = \sum_{A,A'} \int dr dr' \rho_{A,A'}(r, r') |A, r\rangle \langle A', r'|. \quad (5)$$

where r and r' are the collections of the positions of the atoms. The recycling superoperator is given by

$$\begin{aligned} \mathcal{R}[\rho] = & 2 \sum_{i,j} \sum_{A,A'} \int dr dr' \rho_{A,A'}(r, r') \text{Im}[g](\tilde{\mathbf{r}}'_{ij}) \\ & \times \sigma_i^- |A, r\rangle \langle A', r'| \sigma_j^+, \end{aligned} \quad (6)$$

where $\text{Im}[g]$ is the imaginary part of the Green's function, and $\tilde{\mathbf{r}}'_{ij} = \tilde{\mathbf{r}}_i - \tilde{\mathbf{r}}'_j$. The multiplication of the density matrix by the position dependent Green's function in the above equation is responsible for and explains the mechanism of the imparting of momentum and energy to the atoms during the photon emission step. We use a spectral method employing the eigenstates of a truncated position operator $(a + a^\dagger)$ as the basis to calculate this superoperator action. This results in a faster convergence with the number of basis states as done in the appendix of Ref. [22].

C. Green's function

The Green's function in Eq. (4) depends on the underlying geometry of the system. For atoms coupled to a 1D waveguide (assuming no other decay channel), the Green's function has a simple form and leads to coupling given by [15]:

$$g(\mathbf{r}) = i \frac{\gamma_0}{2} \exp(ik_0|\mathbf{r}|), \quad (7)$$

where $k_0 = 2\pi/\lambda_0 = \omega_0/c$ is the wave number of light, λ_0 is the wavelength of light, and c is the speed of light. For a waveguide along the x-axis, $\mathbf{r} = x\hat{x}$ and $|\mathbf{r}| = |x|$ denotes the distance between two atoms in 1D. This function is simple because it is bounded and periodic.

On the other hand, the Green's function for free space is more complicated and given in Eq. (8):

$$g(\mathbf{r}) = i \frac{\gamma_0}{2} \left[h_0^{(1)}(k_0 r) + \frac{3(\hat{r} \cdot \hat{q})(\hat{r} \cdot \hat{q}^*) - 1}{2} h_2^{(1)}(k_0 r) \right] \quad (8)$$

where \hat{q} is the dipole orientation, $r = |\mathbf{r}|$ is the norm of the vector \mathbf{r} , $\hat{r} = \mathbf{r}/r$ is the unit vector along \mathbf{r} , and $h_l^{(1)}(x)$ are the outgoing spherical Hankel functions of angular momentum l ; $h_0^{(1)}(x) = e^{ix}/[ix]$ and $h_2^{(1)}(x) = (-3i/x^3 - 3/x^2 + i/x)e^{ix}$. Unlike the 1D case, this Green's function is non-periodic. Its magnitude decays like $1/r$ at large r , and its real part diverges like $1/r^3$ at small r . In Eq. (4), this leads to infinities in the self-interaction terms $i = j$, and we remove the real part of the Green's function at $i = j$ to avoid the infinities.

The distinction between \mathbf{R}_i and \mathbf{r}_i (see Fig. 1) is important for the description of the motional aspect of the system but also has conceptual consequences for the following reason. The atoms interact through the electromagnetic field. As described in Eq. (4) and in Eqs. (7 and 8), the interaction strength depends on the phase difference of light due to the difference of absolute positions: $k_0|\tilde{\mathbf{r}}_{ij}|$, where k_0 is the wave number of light. This has contribution from the relative positions of the traps, $k_0\mathbf{R}_{ij}$, which is a fixed value. The other contribution comes from $k_0\mathbf{r}_{ij}$, which is a quantum operator that describes the spatial degree of freedom of an atom inside its trap.

In the theoretical limit of infinitely trapped or infinitely massive atoms, this operator can be taken to be fixed, $k_0\mathbf{r}_{ij} = 0$. This approximation is often used in theoretical studies of collective decay. For finite trapping strength, the position operator

$$k_0\mathbf{r}_i = \eta (a_i + a_i^\dagger), \quad (9)$$

where η is the Lamb-Dicke (LD) parameter given by $\eta = k_0 \sqrt{\frac{\hbar}{2m\omega_t}}$. This LD parameter serves two purposes. First, it quantifies the coupling between the internal and vibrational states. The coupling $g(\tilde{\mathbf{r}}_{ij})$ in Eq. (4) can be Taylor expanded in the LD parameter to give terms where the vibrational operators, a_i and a_i^\dagger , are multiplied by the internal operators σ_i^+ and σ_i^- . Second, the LD parameter quantifies the spatial spread of vibrational state of an individual atom. For example, the standard deviation of position divided by λ_0 is equal to $\eta/2\pi$ for the ground vibrational state. Typically, the LD regime is characterized by a spread that is much smaller than the wavelength, corresponding to $\eta \ll 2\pi$.

D. Schrödinger equation

The master equation in Eq. (2) is computationally expensive to solve. In the case of starting in a pure state

of the single excitation subspace with no driving laser, the master equation can be solved more efficiently in two parts: 1) a Schrödinger equation for the electronic excited state that does not depend on the electronic ground state dynamics. 2) a recycling superoperator that accumulates the decayed population in the electronic ground state.

In this paper, we always start the system from a pure state $|\psi(t=0)\rangle = |DS, 0\rangle$, where $|DS\rangle$ is an electronic eigenstate and $|0\rangle$ is the vibrational ground state of all atoms. In this case, the Schrödinger equation is a pure state equation:

$$\frac{d|\psi(t)\rangle}{dt} = \frac{-i}{\hbar} H_{\text{eff}} |\psi(t)\rangle. \quad (10)$$

The magnitude of this state, $\langle\psi(t)|\psi(t)\rangle$ is equal to the probability of being in the excited state, $p(t)$. This probability decays over time due to the non-hermiticity of the effective Hamiltonian. The rate of change of probability is given by

$$\frac{dp(t)}{dt} = \frac{2}{\hbar} \text{Im} \left[\langle\psi(t)| \hat{H}_{\text{int}} |\psi(t)\rangle \right], \quad (11)$$

with a corresponding decay rate defined as $\gamma_d(t) = -\frac{dp(t)}{dt}/p(t)$. The decayed population $1 - p(t)$ goes into the electronic ground state $|g\rangle \langle g|$ where it evolves under the trap term.

E. Observables

The full system time dependent density matrix can be reconstructed as $\rho(t) = \rho_g(t) + \rho_e(t)$, where $\rho_g(t)$ is the decayed density matrix, and $\rho_e(t) = |\psi(t)\rangle \langle\psi(t)|$ is the pure excited state density matrix. However, keeping track of $\rho_g(t)$ is cumbersome, as it is usually a mixed state that evolves under the trap Hamiltonian.

$$\frac{d\rho_g(t)}{dt} = -\frac{i}{\hbar} [H_{\text{trap}}\rho_g(t) - \rho_g(t)H_{\text{trap}}] + \mathcal{R}[\rho_e(t)]. \quad (12)$$

Nevertheless, having the full $\rho(t)$ is rarely needed. We show how various quantities of interest such as the accumulated energy, infidelity, and entanglement entropy can be calculated from the evolved electronic excited state $|\psi(t)\rangle$ alone.

The accumulated energy at time t , $E_R(t) \equiv \langle H_{\text{trap}} \rangle(t)$, can be calculated by adding the energy of the electronic excited state and the electronic ground state $E_e(t) + E_g(t)$. $E_e(t)$ is equal to $\langle\psi(t)| H_{\text{trap}} |\psi(t)\rangle$, and $E_g(t)$ is accumulated over time from the recycling superoperator:

$$E_R(t) = E_e(t) + \int_0^t \text{Tr}\{H_{\text{trap}}\mathcal{R}[|\psi(t)\rangle \langle\psi(t)|]\} dt. \quad (13)$$

For highly subradiant configurations, storing a photon for a long time is of interest [15]. In particular, we wish to store the photon in a state of type $|DS, 0\rangle$, where the electronic part is in a highly subradiant mode, $|DS\rangle$, and

all atoms are in the vibrational ground state, $|0\rangle$. In the early dynamics of such a state ($t \ll 1/\gamma_d$), the decayed population, $\text{Tr}(\rho_g(t))$, is small and the system is mostly in the excited state.

However, due to the coupling between the electronic and vibrational states, the pure electronic eigenmode, $|DS, 0\rangle$, generally turns into a superposition that includes other excited states that have different electronic or vibrational excitations. This leads to decoherence and infidelity in the stored excitation. The infidelity due to the mixing of the internally excited states is a measure of the closeness between the excited state at time t and at time 0 and is given by [23]

$$I(t) = 1 - \sqrt{\langle DS, 0 | \rho^{\text{proj}}(t) | DS, 0 \rangle}, \quad (14)$$

where $\rho^{\text{proj}}(t) = \rho_e(t)/\text{Tr}(\rho_e(t))$. The reason we project the density matrix is to isolate the infidelity due to the mixing of the excited states from the infidelity due to the decay of the excited state. In the context of conditional measurements, if there is no photon detected before time t , the state of the system is $\rho^{\text{proj}}(t)$ and only the infidelity due to the mixing of the excited states is relevant.

In general, the electronic and vibrational parts of the state $\rho_e(t)$ become entangled before the state decays. The entanglement entropy is calculated from the reduced density matrix of the internal states of the atoms $\rho_A(t) = \text{Tr}_V[\rho^{\text{proj}}(t)]$, where Tr_V is the trace over the vibrational states of the atoms. The entanglement entropy is given by [23]

$$S(t) = -\text{Tr}[\rho_A(t)\ln(\rho_A(t))]. \quad (15)$$

One goal of this paper is to identify the conditions under which the entanglement entropy and the infidelity are minimized.

III. RESULTS

In this section, we show the effects of finite traps on the decay, recoil, and decoherence of dark states in quantum emitter arrays. We begin by studying two atoms in a 1D waveguide, where the atoms can be put in a highly subradiant configuration at $d = \lambda_0$ separation. We show that the decay rate is lower bounded by the spread of the wavefunction, and we demonstrate that the decay rate can be significantly affected by the induced forces between the atoms. We calculate the energy imparted to the atoms during the decay and show that this energy could be much larger than the trap energy spacing, $\hbar\omega_t$, when the forces are significant.

We then extend our study to three atoms in a waveguide, where the initially separable system of electronic and vibrational states becomes entangled through the collective decay. We give numerical results and analytic approximations for the amount of infidelity and entropy generated with time. Finally, we extend the decoherence and infidelity treatment of three atoms to many-atom

arrays in free space. We show that the exponentially improved decay rate proposed in Ref. [11] is lower bounded by the spread of the atoms. We also explore a qualitative expression for the dependence of the storage fidelity on the spread, trap frequency, distance between atoms, and number of atoms.

A. Two Atoms in a 1D Waveguide

We begin with the simplest example of highly subradiant states: two atoms in a 1D waveguide. In the single excitation subspace, the symmetrized combination can lead to subradiant or superradiant states when they are separated by a wavelength. The symmetrized electronic states are:

$$|\pm\rangle = \frac{|ge\rangle \pm |eg\rangle}{\sqrt{2}}. \quad (16)$$

The effective Hamiltonian for this system is

$$H_{\text{eff}} = \hbar\omega_t \sum_i a_i^\dagger a_i - \sum_i \frac{i\hbar\gamma_0}{2} \sigma_i^+ \sigma_i^- - \hbar g(\mathbf{R}_{12} + \mathbf{r}_{12}) (\sigma_1^+ \sigma_2^- + \sigma_1^- \sigma_2^+) \quad (17)$$

In the single excitation symmetrized states, the effective Hamiltonian acting on $|\pm\rangle$ becomes [24]:

$$H_{\text{eff}}^\pm = \hbar\omega_t \sum_i a_i^\dagger a_i - \frac{i\hbar\gamma_0}{2} \{1 \pm \exp(i\phi + ik_0\mathbf{r}_{12})\}, \quad (18)$$

where $\phi = k_0d$ is the phase difference due to the separation of the traps.

For fixed point-like atoms located at the center of the traps, the operator $k_0\mathbf{r}_{12}$ is zero, and the decay rate is

$$\gamma_d = \gamma_0 \{1 \pm \cos(\phi)\}, \quad (19)$$

which leads to the constructive or destructive interference depending on ϕ . For fixed point-like atoms, perfect dark states can be achieved by positioning the atoms in the $|-\rangle$ state separated by a multiple of λ_0 (or by an odd multiple of half-wavelength for the $|+\rangle$ state). We investigate the $|-\rangle$ state with integer λ_0 spacing as the dark state, and we use the effective Hamiltonian for the $|-\rangle$ state.

If the atoms are in a non-zero spread ground state of the trap, $|-, 0\rangle$, the decay rate at integer wavelength separation becomes

$$\gamma_d = \gamma_0 \{1 - \exp(-\eta^2)\} \simeq \eta^2 \gamma_0, \quad (20)$$

where the term $\exp(-\eta^2)$ accounts for the non-zero spatial spread of the wavefunction. This term arises from the convolution integral of the position probability distribution with the imaginary part of the Green's function, as in Eq. (11). It prevents the perfect cancellation in Eq.

(20), resulting in a lower bound for the decay rate $\sim \eta^2 \gamma_0$, for small η [18].

For identically trapped atoms in the dark state configuration, the effective Hamiltonian, H_{eff}^- , in Eq. (18) can be decomposed into two components: (1) a center-of-mass Hamiltonian, $H_{\text{cm}} = \hbar\omega_t a_{\text{cm}}^\dagger a_{\text{cm}}$, representing a pure harmonic oscillator with no perturbation, and (2) a relative motion Hamiltonian, H_{rel} , which is a harmonic oscillator perturbed by dipole-dipole interactions:

$$H_{\text{rel}} = \hbar\omega_t a^\dagger a - \frac{i\hbar\gamma_0}{2} \{1 - \exp(ik_0\mathbf{r}_{12})\}, \quad (21)$$

where the non-indexed lowering operator, a , defined as $a = (a_1 - a_2)/\sqrt{2}$, acts on the relative displacement states. Here, $k_0\mathbf{r}_{12}$ can be expressed as $\sqrt{2}\eta(a + a^\dagger)$.

The relative Hamiltonian in Eq. (21) can be further expanded, assuming small η and neglecting terms of order η^3 and higher, as

$$H_{\text{rel}} \approx \hbar\omega_t a^\dagger a + \frac{\hbar\gamma_0}{2} k_0\mathbf{r}_{12} - \frac{i\hbar\gamma_0}{4} (k_0\mathbf{r}_{12})^2 = \hbar\omega_t a^\dagger a + \frac{\hbar\gamma_0\eta}{\sqrt{2}} (a + a^\dagger) - \frac{i\hbar\gamma_0\eta^2}{2} (a + a^\dagger)^2, \quad (22)$$

The terms in this expansion represent the trap of strength ω_t (first term), a linear potential of strength $\gamma_0\eta$ (second term), which pushes the wave packet away from the trap center, and non-uniform decay of strength $\gamma_0\eta^2$ (third term), which deforms the wave packet because the wave function's tails decay faster than its center. Throughout this work, we demonstrate that the relative strength of these terms determines the behavior of decay, recoil, and decoherence in the dark states. It is useful to consider three trap regimes: a *strong trap* regime where the trap dominates the induced forces, $\omega_t \gg \gamma_0\eta$, a *weak trap* regime where the induced forces dominate, $\omega_t \ll \gamma_0\eta$, and an *intermediate trap* regime where the trap is only slightly stronger than the induced forces, $\omega_t \gtrsim \gamma_0\eta$.

The effects of the induced forces and the non-uniform decay become manifest in weak traps. To isolate the effects of the different terms in (Eq. 22), we simulate three cases: 1) The full Hamiltonian as in Eq. (21) with the induced forces present. 2) The Hamiltonian without the induced real (coherent) potential term: $H_{\text{rel}} \rightarrow \hbar\omega_t a^\dagger a - \frac{i\hbar\gamma_0}{2} \{1 - \cos(k_0\mathbf{r}_{12})\}$. 3) The Hamiltonian with the traps center shifted to cancel the linear potential term: $H_{\text{rel}} \rightarrow H_{\text{rel}} - \hbar\gamma_0\eta(a + a^\dagger)/\sqrt{2}$. In other words, we cancel the linear part of the induced potential by adding a linear potential to the Hamiltonian.

The results of the simulations are in Figs. 2, 3, and 4. In these simulations, the mass of the atoms is $m = 2.21 \times 10^{-25}$ kg, and the individual atom decay rate is $\gamma_0 = 10^8$ s $^{-1}$. The internal transition has $\lambda_0 = 1000$ nm, and the trap frequency is $\omega_t = 0.01\gamma_0 = 10^6$ s $^{-1}$ resulting in $\eta \approx 0.1$. The system is initialized in the dark state configuration $|-\rangle |00\rangle$ with λ_0 separation.

In Fig. 2, we plot the time dependent excited state population for the three cases. Initially, all cases exhibit

an exponential decay with a rate of approximately $\gamma_0\eta^2$, but then deviate due to the change of the vibrational wavefunction. For cases where forces are absent or traps are shifted (cases 2 and 3), the decay rate slightly decreases. However, in the presence of forces (case 1), the decay rate greatly increases for $t > 50/\gamma_0$.

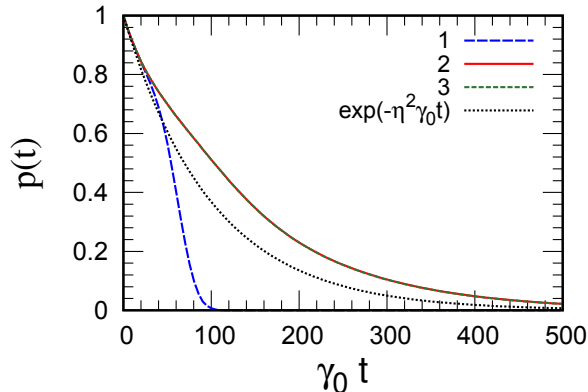


FIG. 2: Decay of the excited population across cases discussed in the text. In all cases, the decay starts out in a similar way. An exponential decay at rate $\gamma_0\eta^2$ is also plotted for reference. Simulation parameters: $\omega_t = 0.01\gamma_0$, spread $\eta \approx 0.1$, initial dark state configuration $|-\rangle|00\rangle$ at λ_0 separation.

The time dependence of the decay rate can be explained by the evolution of the spatial wavefunction. Figure 3 plots the mean position and width of the wavefunction over time. In the absence of forces (case 2) or with shifted traps (case 3), the wavepacket width decreases slightly due to faster decay of the wings, while the center of the wave packet remains nearly unchanged. This leads to a decrease in the standard deviation of position, $\sigma_{x_{12}}$, and thereby a decrease in the decay rate of Fig. 2. With forces present (case 1), the relative wavefunction shifts rightward, which is due to the repulsive interaction between the atoms' individual wavepackets. The shift of the position of the wavefunction changes the relative phase ϕ from the initial value 2π , resulting in a faster decay as per Eq. (19).

The motion of the wavepacket in Fig. 3 not only affects the decay rate but also results in the atoms gaining kinetic and potential energy before they decay. This contributes to the excited state energy term, E_e , discussed in Sec. II E. This term builds up as the atoms are accelerated away from the trap center. This excited state energy is then transferred to the ground state energy term, E_g , as the atoms decay. When the atoms decay, they acquire additional recoil energy due to the emission of the photon. These two effects add up to the total energy of the atoms, E_R . As a consequence of these two contributions, the energy gained by the atoms exhibits qualitatively different behavior based on the trap strength.

In the strong trap regime, $\omega_t \gg \gamma_0\eta$ (or if the induced

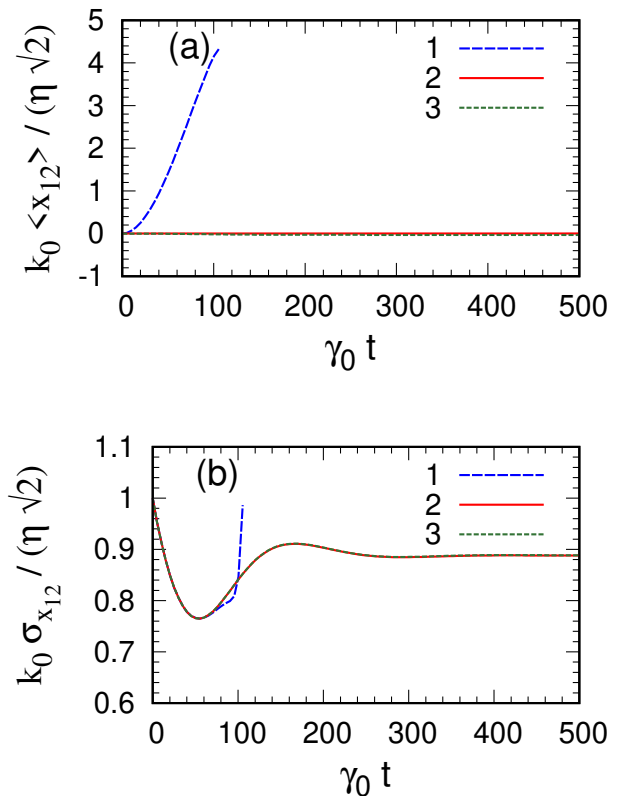


FIG. 3: (a) the time-dependent expectation of the scaled relative position operator $k_0 x_{12}/(\sqrt{2}\eta)$ and (b) its standard deviation $k_0 \sigma_{x_{12}}/(\sqrt{2}\eta)$.

forces are absent or negligible), the induced forces are small, resulting in the excited state gaining minimal energy, $E_e(t) \approx 0$ for all t . In this case, the decay is exponential and the final energy is mostly from the recoil due to the emission of the photon. The total recoil energy of the atoms is inversely proportional to the decay rate, as noted in Ref. [1] leading to

$$E_R = \frac{\gamma_0}{\gamma_d} E_r, \quad (23)$$

where $E_r = \frac{\hbar^2 k_0^2}{2m}$ is the *one-atom* recoil energy coming from momentum conservation during a photon emission from the state $|e\rangle$. The recoil energy in Eq. (23) after photon emission is derived from the recycling term, assuming a stationary initial excited state. For the dark state of two atoms in a 1D waveguide, the decay rate is approximately $\gamma_0\eta^2$, giving a recoil energy of

$$E_R \approx \frac{E_r}{\eta^2} = \hbar\omega_t. \quad (24)$$

On average, a vibrational quantum is generated in this subradiant case in the strong trap regime. In Fig. 4, the motional energy gained by the atoms is shown for

the three cases. When the forces are absent (case 2) or when the traps are shifted (case 3), the final energy is close to $\hbar\omega_t$, with difference $(E_R(\infty) - \hbar\omega_t)$ coming from the narrowing of the wavepacket due to the non-uniform decay. However, with forces present (case 1), the final energy significantly exceeds $\hbar\omega_t$, mostly coming from the wavepacket displacement.

The energy gained by the atoms may be deposited either in the center-of-mass motion, H_{cm} , of the two atoms or in their relative motion, H_{rel} . For symmetric traps, a small fraction of the recoil energy, $E_r/2 = \eta^2 \hbar\omega_t/2$, is deposited in the center-of-mass mode.

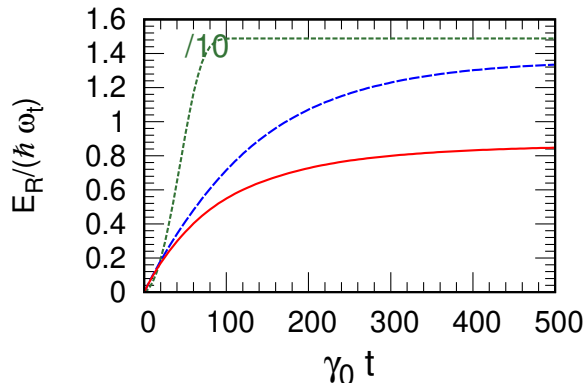


FIG. 4: Energy gained by the atoms. In case 2 without induced potential, the final energy (blue long dashed) is about 1.3 units of the trap level separation, $\hbar\omega_t$. In case 3 with shifted traps, the final energy (red solid) is approximately $0.8\hbar\omega_t$. In case 1 with forces present, the final energy (green short dashed) substantially exceeds $\hbar\omega_t$ and is about $15\hbar\omega_t$. To fit in the same plot, the curve for case 1 has been divided by 10 as annotated.

The energy gained by the atoms and their decay behavior are manifest in the spectrum of the emitted photon [25]. The spectrum can be reconstructed following the ‘input-output’ formalism as in Refs. [26–28]. We calculated the spectrum of the emitted photon for the two atoms in a 1D waveguide in cases 1 and 2. In both cases the spectrum is red shifted on average by the final energy deposited in the atoms, $E_R(\infty)/\hbar$, and its width corresponds to the average decay rate of the subradiant state.

B. Three Atoms in a 1D Waveguide

For a system of two atoms, the dark state $|-\rangle$ is an eigenstate of the effective Hamiltonian. Consequently, this state remains decoupled from the bright state $|+\rangle$ during the decay process, irrespective of atomic motion. This leads to the entanglement entropy $S(t)$, as defined in Eq. (15), remaining identically zero. However, at least two states are needed for a qubit. Therefore, we study a

system of three atoms which can support two dark states.

In the single-excitation subspace, three atoms in a 1D waveguide, separated by λ_0 , form two dark states and one bright state [15, 29, 30]. The dark states can be defined as:

$$|DS_1\rangle = \frac{1}{\sqrt{2}} (|egg\rangle - |gge\rangle), \quad (25)$$

$$|DS_2\rangle = \frac{1}{\sqrt{6}} (|egg\rangle - 2|geg\rangle + |gge\rangle), \quad (26)$$

and the bright state is:

$$|BS\rangle = \frac{1}{\sqrt{3}} (|egg\rangle + |geg\rangle + |gge\rangle). \quad (27)$$

If the atoms are fixed at integer wavelength separation, the dark states remain non-decaying while the bright state decays at a rate of $3\gamma_0$ [15]. When the atoms have a non-zero spread in a vibrational ground state, the dark states decay at rate of $\simeq \eta^2\gamma_0$, and the bright state decays at a rate of $\simeq (3 - 2\eta^2)\gamma_0$ in the Lamb-Dicke regime. Using the two dark states as qubit states allows high fidelity for a duration less than the lifetime ($< 1/(\eta^2\gamma_0)$). The lifetime is long because these subradiant states are almost exact eigenstates of the system and decay at the same, slow rate [29].

While the previous discussion focused on decay dynamics, practical traps introduce coupling between the two dark states due to atomic motion. For example, starting from $|DS_1, 0\rangle$, we observe population transfer to the electronic states $|DS_2\rangle$ and $|BS\rangle$, as shown in Fig. 5. In this simulation, we chose favorable parameters to preserve fidelity: $\eta = 0.01$, $\omega_t = 0.1\gamma_0$, and $d = \lambda_0$. The choice of $\eta = 0.01$ corresponds to an atom 10 times heavier than a Cesium atom, while maintaining the same ω_0 and γ_0 as before.

Unlike the complete decay dynamics in Fig. 2 for two atoms, Fig. 5 only shows the early dynamics where the decayed population, $1-p(t)$, is under 1.4%. For reference, if the atoms are confined to the ground state of the trap, the lifetime $1/\gamma_d$ is approximately $1/(\eta^2\gamma_0) = 10000/\gamma_0$, while we only simulate for $t_f = 100/\gamma_0$. In this time window, the state $|DS_2\rangle$ (summed over all vibrational states) populates up to approximately 1.95% and oscillates with a period close to the trap period $2\pi/\omega_t \approx 62.8/\gamma_0$. The bright state $|BS\rangle$ also populates to a small fraction $\approx 1 \times 10^{-5}$. The simple sinusoidal behavior results because the dipole-dipole interaction couples $|DS_1, 0\rangle$ with $|DS_2\rangle$ in the $n = 1$ subspace, and these states have an energy splitting $\simeq \hbar\omega_t$, see App. A.

This mixing between the states is only possible owing to the coupling between the internal and the vibrational states. In the process of the population transfer from the initial state, there is entanglement entropy ($S(t)$ as defined in Eq. (15)) generated. The entropy is not shown in the figure but is approximately proportional to the population in $|DS_2\rangle$. For example there is a peak in the

entropy at $t \approx 30/\gamma_0$ which corresponds to the time when the population in $|DS_2\rangle$ is at its maximum. This peak is at $S(t) \approx 0.1$ which is small but could affect applications. Like the entropy, the populating $|DS_2\rangle$ causes infidelity, $I(t)$, that is proportional to the population in $|DS_2\rangle$ and also peaks at $t \approx 30/\gamma_0$ at a value approximately 0.01.

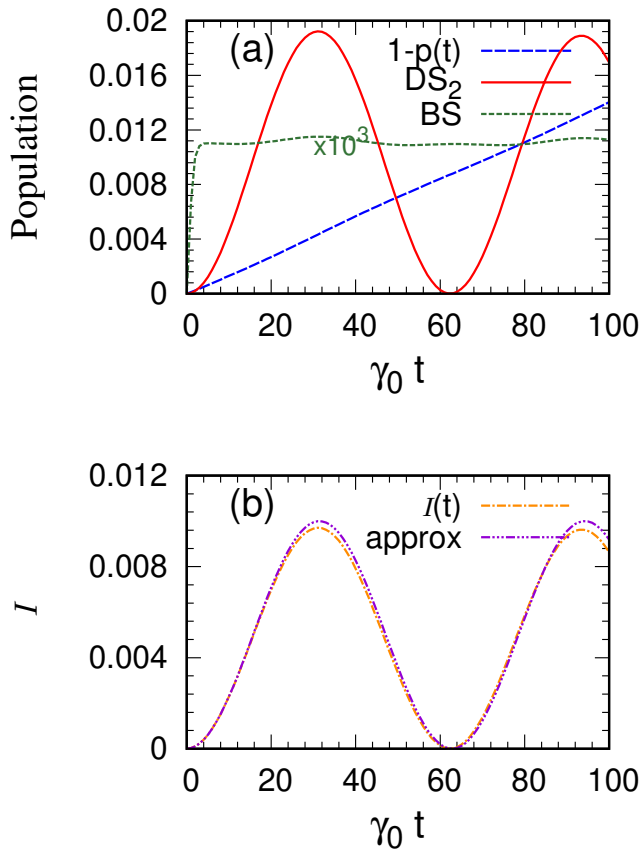


FIG. 5: Early dynamics of three atoms in a 1D waveguide. (a) the decayed population ($1 - p(t)$), the population in $|DS_2\rangle$, as well as the population in $|BS\rangle$ (multiplied by 10^3 for clarity). (b) the infidelity $I(t)$ builds up and oscillates as a proportional amount of $|DS_1\rangle$ is transferred back and forth to $|DS_2\rangle$. An analytical approximation, $0.01 \sin^2(\omega_t t/2)$, for $I(t)$ is derived in App. A. Parameters are $\omega_t = 0.1\gamma_0$ and $\eta = 0.01$.

The oscillation amplitude for the entropy or the infidelity curves can serve as a figure of merit to compare the effects of the trap strength and the induced forces across different system parameters, η and ω_t . In the intermediate or strong trap regime, we found that the amplitude of the oscillations depends on the ratio of the force term to the trap term, similar to the condition for exponential decay for two atoms. Specifically, the infidelity amplitude scales as $\sim (\gamma_0 \eta / \omega_t)^2$. This scaling, derived in Appendix A, arises because the force term, $\gamma_0 \eta$, functions as a coupling in an effective two-level system, while the trap term,

ω_t , serves as a detuning. In the weak trap regime, such as in the case for Fig. 2, the mixing between the internal states is largest, and the entropy, $S(t)$ rapidly reaches a maximum value of $S_{\max} \approx \ln(2)$, which describes a completely mixed effective two-level system. To achieve an order 10^{-4} infidelity (or three nines of fidelity in the language of quantum information) for a case with 3 Cs atoms with the transition $6^2S_{1/2} \leftrightarrow 6^2P_{3/2}$, a relatively strong trap of frequency $\omega_t \approx 2\pi \times 3$ MHz $\approx \gamma_0/2$ is needed.

C. Circular Array of Atoms in Free Space

In this section, we present results for highly subradiant states of atoms interacting in free space, without a waveguide. For the free space case, a highly subradiant configuration of two atoms only occurs at nearly zero separation. For example, for two atoms polarized along the z axis with a separation along the x axis, the atoms need to be placed in the $|-\rangle$ state at $d \approx 0.1\lambda_0$ to achieve a 10-fold decrease from the individual decay rate, $\gamma_d = \gamma_0/10$ [24]. This is impractical due to the rapid increase of induced dipole forces at such close distances. For instance, assuming spread $\eta = 0.02$, a trap frequency $\omega_t \gtrsim \gamma_0$ is necessary to prevent the atoms from colliding due to the attractive dipole-dipole forces. An alternative approach to suppressing the decay rate, without going to very small separations, is to arrange multiple atoms in a regular array with separation $d < 0.5\lambda_0$ [11], which is the main focus of this section.

For a large number, N , of point-like atoms arranged in a circular array in free space, the decay rate of the most subradiant eigenstate can be made very small by increasing N , provided that the separation between atoms is less than $\lambda_0/2$ [11]. In the infinite limit $N \rightarrow \infty$, the decay rates of many eigenstates approach zero. These eigenstates are electronic (spin) waves with different wavenumbers k . When k exceeds the free-space wavenumber k_0 , the radiation must be evanescent perpendicular to the array, resulting in guided modes around the ring that are completely dark. For finite even N , the most subradiant eigenmode is the one with the largest k which is equal to π/d . This state which we call $|DS_{\min}\rangle$ is an equal superposition of all single excitation states with alternating signs. The decay rate of this state, γ_{\min} , decreases exponentially as $\exp(-N/N_0)\gamma_0$, where N_0 is a constant that depends on the interatom distance, d . The resulting highly subradiant states of the ring are promising for the storage of photons and quantum information.

If the atoms are spread in the ground state of a trapping potential, as shown in Fig. 1, the decay rate of the most subradiant state has two primary contributions: (1) the finite size of the array, which scales like $\sim \exp(-N/N_0)\gamma_0$, and (2) the finite spread of the atoms' wavefunction, which contributes a factor of $\sim \eta^2\gamma_0$. At sufficiently large N , γ_{\min} reaches an asymptotic value dominated by the atomic spread, γ_{spread} , as illustrated

in Fig. 6 and derived in Appendix B. However, as d increases, more atoms are required to reach this spread-dominated regime. In the case in Fig. 6, the atoms are taken to have position spread in the plane of the atoms (x-y plane), but no spread in the perpendicular direction. Also, their polarization is perpendicular to the plane of the atoms ($\hat{q} = \hat{z}$). In this case, $\gamma_{spread} \approx 0.8\eta^2\gamma_0$. If the polarization was circular around the z-axis ($\hat{q} = (\hat{x} + i\hat{y})/\sqrt{2}$) instead, the limiting decay rate, γ_{spread} , becomes $0.6\eta^2\gamma_0$.

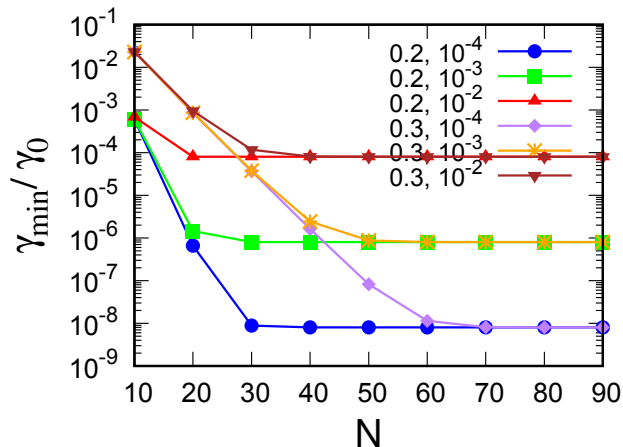


FIG. 6: Decay rate of the most subradiant eigenstate for N atoms, confined to the vibrational ground state ($n = 0$), in a ring configuration in the x-y plane with $\hat{q} = \hat{z}$. The legends represent the parameter pair $d/\lambda_0, \eta$. The decay rate decreases exponentially with N until reaching a minimum value controlled by the squared spread, $\approx 0.8\eta^2\gamma_0$, at large N .

These minimum decay rates were calculated by diagonalizing the non-Hermitian effective Hamiltonian (restricted to $n_{max} = 0$ so all atoms are in the ground vibrational state). An alternative way is to utilize the ring symmetry [31] which results in the spin waves always being the eigenmodes of the system independent of η and d . In this way, γ_{min} is equal to $2 \text{Im}\{\langle DS_{min} | H_{eff} | DS_{min} \rangle\} / \hbar$. A third way of calculation is to use statistical methods. In the calculation of γ_{min} , we found that having vibrational ground states is approximately equivalent to point-like atoms that have a Gaussian position distribution equal to that of the vibrational ground state. Computationally, we sample a position configuration from the Gaussian distribution, which gives a particular H_{eff} , and calculate $2 \text{Im}\{\langle DS_{min} | H_{eff} | DS_{min} \rangle\} / \hbar$. We repeat this process many times and average the results.

Similar to the case of three atoms, forces between atoms in the ring induce entanglement between their internal and vibrational degrees of freedom. Figure 7 shows the mixing dynamics starting from $|DS_{min}, 0\rangle$. The parameters used are $\omega_t = 0.1\gamma_0$, $\eta = 0.01$, $d = 0.3\lambda_0$, $\hat{q} = \hat{z}$, and $N = 30$. In the time shown, approximately

0.7% of the population has decayed. A small fraction, about 0.04%, transfers from the initial internal state to other internal states in the first vibrational mode, $n = 1$, (summed over the all the internal states). This process generates entanglement entropy $S(t)$ and produces infidelity $I(t)$. Compared to the 3 atoms case in Fig. 5 which has the same η and ω_t , the infidelity here is much smaller, of order 10^{-4} , compared to 10^{-2} for the waveguide atoms. This can be explained by the magnitude of the induced forces between the atoms. For a waveguide at λ_0 separation, the force is $\hbar\gamma_0 k_0$. For free space at $d = 0.3\lambda_0$ and when the polarization is perpendicular to the plane of the atoms, the force is much smaller, approximately $0.03\hbar\gamma_0 k_0$. This is a particularly useful arrangement for storing quantum information, as the decay rate is small and the induced forces are weak. The force stays small for d/λ_0 in the range from approximately 0.25 to 0.5 but increases rapidly for smaller d , as later indicated in Fig. 8. For several other polarization directions, the induced force was found to be larger.

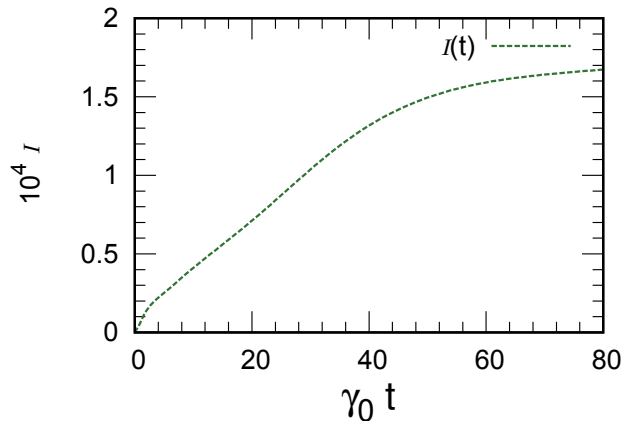


FIG. 7: Similar to Fig. 5(b), the evolution of the most subradiant internal eigenstate for N atoms in a ring configuration, with motion initialized in the ground state of the trap, $|DS_{min}, n = 0\rangle$. Population transfers from the initial internal state to other internal states in the first vibrational mode $n = 1$, leading to increasing infidelity between the evolved state and the initial state, $I(t)$. Parameters: $\omega_t = 0.1\gamma_0$, $\eta = 0.01$, $d = 0.3\lambda_0$, $N = 30$, $\hat{q} = \hat{z}$.

Unlike the periodic mixing seen for three atoms in Fig. 5, the mixing here is not periodic at early times. The lack of periodicity can be explained by the change of energy splitting between the interacting states. For atoms in a waveguide, the splitting is ω_t , which causes oscillations with frequency close to ω_t . While being absent in a waveguide at $d = \lambda_0$, another contribution to the splitting comes from the Lamb shift due the collective coupling in free space at $d = 0.3\lambda_0$. The Lamb shift in this case is approx $-0.25\gamma_0$ for the initial state and $-0.32\gamma_0$ for a typical strongly interacting state in a higher vibrational mode. This uneven Lamb shift causes the energy

splitting between the interacting states to diminish from $\omega_t = 0.1\gamma_0$ (the trap splitting) to only $\approx 0.03\gamma_0$. This results in a slower oscillation and a revival time longer than the time window shown in Fig. 7.

Due to the increasing size of the Hilbert space with N , this simulation uses a restricted vibrational Hilbert space allowing at most one atom to vibrate in one direction at a time. Due to the large number of states in these calculations, we did not check the validity of this vibrational restriction. However, this restriction was checked for validity in the case of 3 atoms in Fig. 5, which was relatively easier to perform due to the fewer number of states. We found that the errors in the populations to be less than 0.1% between this restriction and a convergent calculation that used $N_{vib} = 5$. The errors were even smaller for cases with larger ω_t or smaller η . This suggests that such restriction results in a good approximation in the intermediate trapping regime where vibrational excitations in the $n = 1$ state are less than $\sim 10\%$. Further details of the equations and approximations used are given in the App. B.

1. Trends with Different Parameters

To analyze how infidelity depends on various parameters (N, d, η, ω_t), we consider two approaches. One method involves direct simulations, as in Fig. 7. Unlike the dynamics of the 3 atoms in Fig. 5, these dynamics are not periodic over the observed time range, and infidelity lacks a simple scalar measure in this setting. An alternative approach uses diagonalization of the effective Hamiltonian with and without the force term. Without the induced forces, our initial state, $|DS_{\min}, n = 0\rangle$, is an eigenstate that remains the same with high fidelity for $t < 1/\gamma_{\min}$. With the force term, this state is no longer an exact eigenstate. First, we calculate the eigenstates of H_{eff} including the coupling due to the forces. We then identify the eigenstate $|\zeta\rangle$ that has the highest overlap with $|DS_{\min}, n = 0\rangle$. Finally, the infidelity between these two states captures the effect of the induced forces and is defined as

$$I = 1 - \sqrt{|\langle \zeta | DS_{\min}, n = 0 \rangle|^2}. \quad (28)$$

Consistent with previous findings in waveguide-coupled atoms, the infidelity exhibits a quadratic dependence on η and decreases as $(\omega_t/\gamma_0)^{-2}$ for sufficiently large ω_t . However, as N varies, the infidelity remains within the same order of magnitude, displaying only minor fluctuations.

As the interatomic distance d decreases, there are stronger induced forces, leading to increased infidelity, as illustrated in Fig. 8. Notably, the magnitude of induced forces depends on the polarization direction. For instance, in the case of linear polarization along \hat{z} , the induced forces are weaker than those observed for circular polarization along $\hat{q} = (\hat{x} + i\hat{y})/\sqrt{2}$. Consequently,

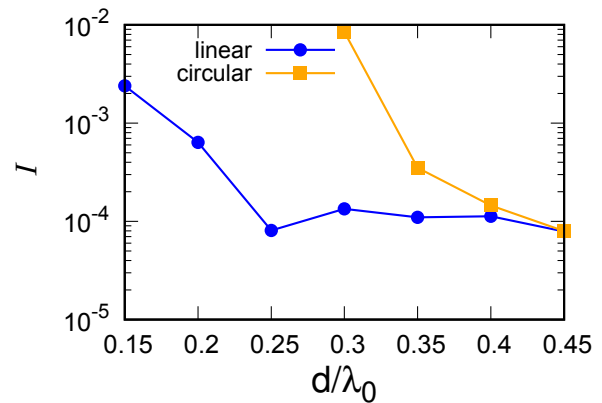


FIG. 8: Infidelity, I , versus interatom separation, d , for linear polarization, $\hat{q} = \hat{z}$, and circular polarization, $\hat{q} = (\hat{x} + i\hat{y})/\sqrt{2}$. Parameters: $\omega_t = 0.1\gamma_0$, $\eta = 0.01$, $N = 20$.

the infidelity is significantly higher for the circular polarization case, as shown in Fig. 8. At $d = 0.3\lambda_0$, for example, the infidelity is on the order of 10^{-4} for perpendicular polarization, whereas it increases to 10^{-2} for circular polarization.

These trends can be explained by the competition between the trap term and the force term, which scales as $\eta \text{Re}(g_\phi)$, where g_ϕ is the derivative of the coupling relation in Eq. (8) with respect to the phase difference $\phi = k_0 r$ evaluated at a neighbor separation $\mathbf{r} = \mathbf{R}_1 - \mathbf{R}_2$. The overall trend of the infidelity can be summarized as:

$$I \sim \left(\frac{\eta \text{Re}(g_\phi)}{\omega_t} \right)^2. \quad (29)$$

This scaling agrees with a perturbation theory argument given the matrix elements coupling the vibrational ground states to the first vibrational states in Eq. (B2) in Appendix B and energy splitting of order $\hbar\omega_t$.

The analysis in this section is performed under the same restriction in Fig. 7: at most one direction of one atom is in the $n = 1$ state at a time. All the data points in the figures are in the perturbative regime where the $n = 1$ population is $\ll 10\%$. Outside this perturbative regime (for example in weak traps or at small d where the induced forces are large), the $n = 1$ restriction may not be valid and the infidelity is usually much larger than the values shown in in Fig. 8, challenging the storage of quantum information in the dark states.

A similar analysis for atoms arranged in a line, instead of a ring, reveals trends closely resembling the circular array case, with one key difference: for N atoms in a line, the decay rate of the most subradiant state scales as $1/N^3$ instead of exponentially [15], with radiance mostly coming from the edges of the array. Like the ring configuration, decay is eventually dominated by atomic spread at large N .

IV. CONCLUSION

In this work we expanded on the calculations of the decay mechanism and the recoil energy of dark states introduced in Refs. [1, 20]. We showed that when the trap is strong, a dark state of atoms in a waveguide has a minimum decay rate scaling like $\eta^2\gamma_0$. Furthermore, after the decay the atoms receive a significant recoil proportional to the lifetime of the excitation. In the strong trap regime, the recoil energy is equal to one harmonic energy level separation, $\hbar\omega_t$, which is concentrated mostly in the relative vibrational mode of the two atoms. This recoil might cause severe heating of the atoms that would require additional cooling steps each time a photon is emitted from a dark state of an atomic array [18].

We also showed that weakly trapped atoms can suffer from the induced forces during the decay. The forces can have detrimental effects by either deforming or moving the motional wavefunction from the dark state configuration leading to accelerated decay. In this case, the atoms receive significant amounts of vibrational energy from the induced forces during the decay. In a 1D waveguide, these could be orders of magnitude bigger than the harmonic level separation. To quantify when the induced forces become important, we showed that for a 1D waveguide a large ratio of $\omega_t/\eta\gamma_0$ is required to maintain the exponential decay and alleviate the effects of the forces. This can be achieved by either having stronger traps or more massive emitters.

Expanding on the idea of storing photons in the collective eigenstates of atoms on a ring as introduced in Ref. [15], we showed that the exponential improvement of the decay rate with the number of atoms N is eventually limited by the spread of the atoms which is $\sim \eta^2\gamma_0$. Furthermore, we explored the infidelity and entanglement due to the induced forces. We showed that the infidelity is proportional to the square of the ratio of the induced forces to the trap frequency. These results have implications on the design of quantum memories and atom array experiments.

Data plotted in the figures is available at [32].

ACKNOWLEDGMENTS

This work was supported by the National Science Foundation under Award No. 2109987-PHY and 2410890-PHY. We thank Deepak Suresh for helpful discussions.

Appendix A: 3 atoms state interactions

In this appendix, we derive a scaling relation for the decoherence of the atoms in the 1D waveguide assuming an intermediate trapping regime, where the trap is strong enough to limit the vibrational excitations to $n_{max} = 1$. For 3 atoms with equal masses and trap frequency and

separation of λ_0 , the system possesses a parity symmetry that simplifies the dynamics of the Hamiltonian in Eq. (4). This parity symmetry is realized by reflecting the atoms (both electronic and vibrational) around the center of the array. For N atoms, this is realized by swapping the electronic operators $\sigma_i \leftrightarrow \sigma_{N-i}$ and the vibrational operators $\mathbf{r}_i \leftrightarrow -\mathbf{r}_{N-j}$. This symmetry leaves the Hamiltonian invariant, and as a result, the Hilbert space can be divided into two sectors that do not interact, the sectors with odd and even parity of the combined internal and vibrational degrees of freedom.

In the $n_{max} = 1$ approximation, there are 4 allowed vibrational states $|n_1n_2n_3\rangle \in \{|000\rangle, |100\rangle, |010\rangle, |001\rangle\}$. The other higher vibrational states can be ignored because their coupling to the initial state is of order $\mathcal{O}(\eta^2)$ which is much smaller than the coupling to the one-vibration states (of order $\mathcal{O}(\eta)$). The one-vibration states can be symmetrized just like for the electronic states.

The symmetrized states are given by

$$\begin{aligned} |0\rangle &= |000\rangle \\ |V_1\rangle &= \frac{1}{\sqrt{3}}(|100\rangle + |010\rangle + |001\rangle), \\ |V_2\rangle &= \frac{1}{\sqrt{6}}(|100\rangle - 2|010\rangle + |001\rangle), \\ |V_3\rangle &= \frac{1}{\sqrt{2}}(|100\rangle - |001\rangle). \end{aligned} \quad (\text{A1})$$

With respect to the spatial parity transformation, $\mathbf{r}_i \leftrightarrow -\mathbf{r}_{N-j}$, the states $|0\rangle$ and $|V_3\rangle$ have even parity while the states $|V_1\rangle$ and $|V_2\rangle$ have odd parity. This can be achieved by applying this transformation on the product states. For example, the state $|001\rangle$ is sent to $-|100\rangle$. In this way, the full Hilbert space breaks into the two subspaces. Because we start in the $|DS_1\rangle|0\rangle$ state, the relevant sector is spanned by $\{|DS_1\rangle|0\rangle, |DS_1\rangle|V_3\rangle, |DS_2\rangle|V_1\rangle, |DS_2\rangle|V_2\rangle, |BS\rangle|V_1\rangle, |BS\rangle|V_2\rangle\}$ which have an odd parity of the full system symmetry. The other states have even parity and do not couple to the initial state.

In our case, there is another simplifying symmetry. Since the forces are pairwise equal in magnitude and opposite in directions, the net force on all atoms is zero resulting in the center of mass vibrational mode ($|V_1\rangle$) separating from the relative modes ($|V_2\rangle$ and $|V_3\rangle$). In this way, the dynamics of the odd sector could be reduced to a Hamiltonian which in the $\{|DS_1\rangle|0\rangle, |DS_1\rangle|V_3\rangle, |DS_2\rangle|V_2\rangle, |BS\rangle|V_2\rangle\}$ basis is (to η order)

$$\frac{H_{\text{odd}}}{\hbar} = \begin{pmatrix} 0 & \frac{\eta\gamma_0}{\sqrt{2}} & \frac{\eta\gamma_0}{\sqrt{2}} & \frac{-\eta\gamma_0}{2} \\ \frac{\eta\gamma_0}{\sqrt{2}} & \omega_t & 0 & 0 \\ \frac{\eta\gamma_0}{\sqrt{2}} & 0 & \omega_t & 0 \\ \frac{-\eta\gamma_0}{2} & 0 & 0 & \omega_t - \frac{3i\gamma_0}{2} \end{pmatrix}. \quad (\text{A2})$$

Note that the terms responsible for the decay of the sub-radiant states are omitted because they are of order (η^2) .

Because we are interested in the early time dynamics, the decayed population is small and can be ignored.

A simpler model can be obtained from ignoring the bright state that only populates in a tiny fraction and decays at fast rate as in Fig. 5. The other states $|DS_1\rangle|V_3\rangle, |DS_2\rangle|V_2\rangle$ behave symmetrically with respect to the $|DS_1\rangle|0\rangle$ and can be further symmetrized to obtain the 2 level Hamiltonian in the $\{|DS_1\rangle|0\rangle, |S\rangle\}$ basis where $|S\rangle$ is the symmetric superposition of $|DS_1\rangle|V_3\rangle$ and $|DS_2\rangle|V_2\rangle$.

$$\frac{H_{2\text{-level}}}{\hbar} = \begin{pmatrix} 0 & \eta\gamma_0 \\ \eta\gamma_0 & \omega_t \end{pmatrix}. \quad (\text{A3})$$

This simple Hamiltonian captures the essential entanglement dynamics in early time. It resembles the Rabi oscillation model where ω_t is the detuning, and $\eta\gamma_0$ is the driving Rabi frequency. When the driving Rabi frequency is small the population of the excited state in early time can be found analytically to be

$$P_S(t) \approx 4 \frac{\eta^2 \gamma_0^2}{\omega_t^2} \sin^2\left(\frac{\Omega t}{2}\right), \quad (\text{A4})$$

where $\Omega = \sqrt{\eta^2 \gamma_0^2 + \omega_t^2}$ is the beating frequency. Ω can be approximated as ω_t for small η , in the intermediate or strong trap regime. Since the state $|S\rangle$ has equal amounts of DS_1 and DS_2 that are in different vibration modes, the system becomes entangled. The amount of population in $|DS_2\rangle$ is given by $P_{DS_2}(t) = P_S(t)/2$.

The resulting fidelity is approximately equal to the classical population fidelity $\sum_i \sqrt{p_i q_i}$ for two distributions p_i and q_i . In our case we have two states starting from $p_1 = 1, p_2 = 0$ and at time t the populations become $q_1 = 1 - q_2, q_2 = P_{DS_2}(t)$. The resulting fidelity is thus $\sqrt{1 - P_{DS_2}(t)}$ in early time. For small excited population, the infidelity becomes approximately $P_{DS_2}(t)/2$ which is the case for the simulation in fig. 5, where the infidelity is close to 1% at its peak. The resulting entanglement entropy is also approximately proportional to $P_S(t)$, although with a different proportionality factor.

Appendix B: Equations and approximations for a circular array of atoms

In this appendix, we give the approximations to simulate the atoms on the ring. The ring is assumed to be in the x - y plane with atoms polarized linearly or circularly in z direction. The locations of the centers of the traps are at $\mathbf{R}_j = \langle X_j, Y_j \rangle = \langle r \cos(j\theta), r \sin(j\theta) \rangle$, where $\theta = 2\pi/N$ and the radius r is equal to $d/(2 \sin(\theta/2))$.

In the intermediate trapping regime, $\omega_t/\gamma_0 \gtrsim \eta$, the forces are strong enough to populate the first vibrationally excited state, $n = 1$, but not strong enough to populate higher vibrationally excited states. Therefore, we obtain a computationally feasible Hilbert space by restricting the vibrations to at most one atom vibrating in one direction at a time. In this case, a vibrationally

excited $|V\rangle \in \{a_{l,i}^\dagger |0\rangle\}$, where i is an index for the atoms and l is either x or y . For simplicity, the atoms have infinite trap and zero spread in the z -direction. The number of vibrational states, N_{vib} , is $2N + 1$, where N is the number of atoms. In addition to this Hilbert state restriction, we work in the LD regime, where we only keep terms up to to the dominant η order for the coupling between the different states and up to the dominant η^2 order for decay rates.

With the polarization described above, the Green's function in equation (8) simplifies to a function of the phase: $g(\mathbf{r}) = f(\phi)$, where $\phi = k_0 r = k_0 \sqrt{x^2 + y^2}$. The relevant matrix elements of the interaction Hamiltonian are given by

$$\begin{aligned} & \langle g, 0 | \sigma_i^- H_{\text{int}} \sigma_j^+ | g, 0 \rangle \\ &= -\hbar \left\{ f(\phi_{ij}) + \eta^2 \left[f''(\phi_{ij}) + \frac{f'(\phi_{ij})}{\phi_{ij}} \right] \right\}, \end{aligned} \quad (\text{B1})$$

for the ground vibrational states. Here, $\phi_{ij} = k_0 \sqrt{(X_i - X_j)^2 + (Y_i - Y_j)^2}$. Note there is an exception to the above rule for $i = j$, in which case the matrix element is equal to $-i\hbar\gamma_0/2$. There is a contribution from the point-like atoms (the first term) and the spread of the atoms of order η^2 (the second term). The matrix elements connecting the ground and first vibrational states are given by

$$\begin{aligned} & \langle g, 0 | \sigma_i^- a_{x,k} H_{\text{int}} \sigma_j^+ | g, 0 \rangle \\ &= -\hbar\eta \frac{k_0 X_{ij} f'(\phi_{ij})}{\phi_{ij}} (\delta_{ik} - \delta_{jk}), \end{aligned} \quad (\text{B2})$$

and similarly for the y direction. The matrix block (connecting all internal states) for an excited vibrational state is similar to the $n = 0$ in Eq. (B1), but with the spread factor of $(3/2)\eta^2$ instead of η^2 (because the first vibrational state is more spread out than the ground state). The form of the function f is relatively complicated, so we calculate the derivatives numerically using finite differences.

The system of the atoms on the ring exhibits a high degree of symmetry (Dihedral group of order N). As a result, it can be shown that the eigenstates of the system are spin waves when restricting to the $n = 0$ subspace [31]. For example, for even N the most subradiant state $|DS_{\text{min}}\rangle$ is a spin wave with wave number $k_{\text{min}} = \pi/d$.

$$|DS_{\text{min}}\rangle = \frac{1}{\sqrt{N}} \sum_{j=1}^N \exp(ik_{\text{min}}jd) \sigma_j^+ |g, 0\rangle. \quad (\text{B3})$$

The eigenvalue associated with this state results in the

minimum decay rate of the system.

$$\begin{aligned}\gamma_{min} &= \frac{2}{\hbar} \text{Im} \langle DS_{min} | H_{\text{int}} | DS_{min} \rangle \\ &= 2 \sum_{j=1}^N (-1)^j \text{Im} \left\{ f(\phi_{1j}) + \eta^2 \left[f''(\phi_{1j}) + \frac{f'(\phi_{1j})}{\phi_{1j}} \right] \right\},\end{aligned}\quad (\text{B4})$$

As found out in Ref. [11], the contribution of the point-like atoms (first term) decreases exponentially with the number of atoms. The contribution from the spread of the atoms is given by

$$\begin{aligned}\gamma_{\text{spread}} &= 2\eta^2 \sum_{j=1}^N (-1)^j \text{Im} \left[f''(\phi_{1j}) + \frac{f'(\phi_{1j})}{\phi_{1j}} \right] \\ &\stackrel{N \rightarrow \infty}{\approx} 0.8\gamma_0\eta^2,\end{aligned}\quad (\text{B5})$$

which is independent of d at large N . The result above holds for a transition dipole moment that is perpendicular to the plane of the array, $\hat{q} = \hat{z}$. For a circular polarized transition, $\hat{q} = (\hat{x} + i\hat{y})/\sqrt{2}$, the limiting decay rate changes to $0.6\gamma_0\eta^2$. The constancy of the decay rate at large N and its independence of d is due to the form of the Green's function and its derivatives. These functions have a dominant term at large atom separation, R_{ij} , which is a sinc function, $\sin(\phi_{ij})/\phi_{ij}$. The alternating sum in Eq. (B5) of this function has a flat behavior at large N for all $d < 0.5\lambda_0$.

-
- [1] Deepak A Suresh and F. Robicheaux, "Photon-induced atom recoil in collectively interacting planar arrays," *Phys. Rev. A* **103**, 043722 (2021).
- [2] P-O Guimond, A Grankin, DV Vasilyev, B Vermersch, and P Zoller, "Subradiant bell states in distant atomic arrays," *Phys. Rev. Lett.* **122**, 093601 (2019).
- [3] HH Jen, "Photon-mediated dipole-dipole interactions as a resource for quantum science and technology in cold atoms," arXiv preprint arXiv:2410.20665 (2024).
- [4] Robert H Dicke, "Coherence in spontaneous radiation processes," *Phys. Rev.* **93**, 99 (1954).
- [5] Michel Gross and Serge Haroche, "Superradiance: An essay on the theory of collective spontaneous emission," *Phys. Rep.* **93**, 301–396 (1982).
- [6] M Gross, C Fabre, P Pillet, and S Haroche, "Observation of near-infrared dicke superradiance on cascading transitions in atomic sodium," *Phys. Rev. Lett.* **36**, 1035 (1976).
- [7] Marlan O Scully, "Collective lamb shift in single photon dicke superradiance," *Phys. Rev. Lett.* **102**, 143601 (2009).
- [8] J Pellegrino, R Bourgain, Stephan Jennewein, Yvan RP Sortais, Antoine Browaeys, SD Jenkins, and J Ruostekoski, "Observation of suppression of light scattering induced by dipole-dipole interactions in a cold-atom ensemble," *Phys. Rev. Lett.* **113**, 133602 (2014).
- [9] Sudhakar Prasad and Roy J Glauber, "Polarium model: Coherent radiation by a resonant medium," *Phys. Rev. A* **61**, 063814 (2000).
- [10] RG DeVoe and RG Brewer, "Observation of superradiant and subradiant spontaneous emission of two trapped ions," *Phys. Rev. Lett.* **76**, 2049 (1996).
- [11] Ana Asenjo-Garcia, M Moreno-Cardoner, Andreas Albrecht, HJ Kimble, and Darrick E Chang, "Exponential improvement in photon storage fidelities using subradiance and "selective radiance" in atomic arrays," *Phys. Rev. X* **7**, 031024 (2017).
- [12] David Plankensteiner, Christian Sommer, Helmut Ritsch, and Claudiu Genes, "Cavity antiresonance spectroscopy of dipole coupled subradiant arrays," *Phys. Rev. Lett.* **119**, 093601 (2017).
- [13] A Grankin, PO Guimond, DV Vasilyev, B Vermersch, and P Zoller, "Free-space photonic quantum link and chiral quantum optics," *Phys. Rev. A* **98**, 043825 (2018).
- [14] L Ruks, KE Ballantine, and J Ruostekoski, "Negative refraction of light in an atomic medium," arXiv preprint arXiv:2412.03622 (2024).
- [15] Ana Asenjo-Garcia, JD Hood, DE Chang, and HJ Kimble, "Atom-light interactions in quasi-one-dimensional nanostructures: A green's-function perspective," *Phys. Rev. A* **95**, 033818 (2017).
- [16] Ephraim Shahmoon, Dominik S Wild, Mikhail D Lukin, and Susanne F Yelin, "Cooperative resonances in light scattering from two-dimensional atomic arrays," *Phys. Rev. Lett.* **118**, 113601 (2017).
- [17] Robert J Bettles, Simon A Gardiner, and Charles S Adams, "Enhanced optical cross section via collective coupling of atomic dipoles in a 2d array," *Phys. Rev. Lett.* **116**, 103602 (2016).
- [18] Oriol Rubies-Bigorda, Raphael Holzinger, Ana Asenjo-Garcia, Oriol Romero-Isart, Helmut Ritsch, Stefan Ostermann, Carlos Gonzalez-Ballester, Susanne F Yelin, and Cosimo C Rusconi, "Collectively enhanced ground-state cooling in subwavelength atomic arrays," arXiv preprint arXiv:2405.18482 (2024).
- [19] Cosimo C Rusconi, Tao Shi, and J Ignacio Cirac, "Exploiting the photonic nonlinearity of free-space subwavelength arrays of atoms," *Phys. Rev. A* **104**, 033718 (2021).
- [20] Deepak A Suresh and F. Robicheaux, "Atom recoil in collectively interacting dipoles using quantized vibrational states," *Phys. Rev. A* **105**, 033706 (2022).
- [21] Ephraim Shahmoon, Mikhail D Lukin, and Susanne F Yelin, "Collective motion of an atom array under laser illumination," in *Advances In Atomic, Molecular, and Optical Physics*, Vol. 68 (Elsevier, 2019) pp. 1–38.
- [22] F. Robicheaux, "Spatial averaging for light reflection and transmission through cold-atom arrays," *Phys. Rev. A* **111**, 013711 (2025).
- [23] Michael A Nielsen and Isaac L Chuang, *Quantum computation and quantum information* (Cambridge university press, 2010).

- [24] Beatriz Olmos and Igor Lesanovsky, “Hybrid sub- and superradiant states in emitter arrays with quantized motion,” arXiv preprint arXiv:2502.01428 (2025).
- [25] Rodney Loudon, *The quantum theory of light* (OUP Oxford, 2000).
- [26] Crispin W Gardiner and Matthew J Collett, “Input and output in damped quantum systems: Quantum stochastic differential equations and the master equation,” *Phys. Rev. A* **31**, 3761 (1985).
- [27] Tommaso Caneva, Marco T Manzoni, Tao Shi, James S Douglas, J Ignacio Cirac, and Darrick E Chang, “Quantum dynamics of propagating photons with strong interactions: a generalized input–output formalism,” *New J. Phys.* **17**, 113001 (2015).
- [28] Alexandra S Sheremet, Mihail I Petrov, Ivan V Iorsh, Alexander V Poshakinskiy, and Alexander N Poddubny, “Waveguide quantum electrodynamics: Collective radiance and photon-photon correlations,” *Rev. Mod. Phys.* **95**, 015002 (2023).
- [29] Vanessa Paulisch, HJ Kimble, and Alejandro González-Tudela, “Universal quantum computation in waveguide qed using decoherence free subspaces,” *New J. Phys.* **18**, 043041 (2016).
- [30] Oriol Rubies-Bigorda, Stuart J Masson, Susanne F Yelin, and Ana Asenjo-Garcia, “Deterministic generation of photonic entangled states using decoherence-free subspaces,” arXiv preprint arXiv:2410.03325 (2024).
- [31] Nadav Antman Ron, Maor Carmi, and Rivka Bekenstein, “Atom-atom entanglement generation via collective states of atomic rings,” *Phys. Rev. Res.* **6**, L042051 (2024).
- [32] “Data for: Effects of finite trapping on the decay, recoil, and decoherence of dark states of quantum emitter arrays, a permanent doi link to the data used in the figures will be provided here once the referreeing process is complete and the figures are in final form.” <https://doi.org/10.4231/????????>